DEVELOPMENTAL BIOLOGY 85, 446-462 (1981)

The Mechanical Basis of Morphogenesis

I. Epithelial Folding and Invagination

G. M. ODELL,[1] G. OSTER, P. ALBERCH, AND B. BURNSIDE

University of California, Berkeley, California 94720

Received May 27, 1980; accepted in revised form January 27, 1981

We present a mechanical model for the morphogenetic folding of embryonic epithelia based on hypothesized mechanical properties of the cellular cytoskeleton. In our model we consider a simple cuboidal epithelium whose cells are joined at their apices by circumferential junctions; to these junctions are attached circumferential arrays of microfilament bundles assembled into a "purse string" around the cell apex. We assume that this purse string has the following property: if its circumference is increased beyond a certain threshold, an active contraction is initiated which "draws the purse-string" and reduces the apical circumference of the cell to a new, shorter, resting length. The remainder of the cell is modeled as a visoelastic body of constant volume. Clearly contraction in one cell could stretch the apical circumferences of neighboring cells and, if the threshold is exceeded, cause them "to fire" and contract. The objective of this paper is to demonstrate that our model, based on the local behavior of individual cells, generates a propagating contraction wave which is sufficient to explain the globally coherent morphogenetic infolding of a wide variety of embryonic epithelia. Representative computer simulations, based on the model, are presented for the initial gastrulation movements of echinoderms, neural tube formation in urodele amphibians, and ventral furrow formation in *Drosophila*.

1. INTRODUCTION

In this paper we initiate a study of the mechanical aspects of morphogenesis. In particular, we shall present a model for the folding and movement of cell sheets which we will apply to certain elementary types of gastrulation and neurulation.

It has long been known that global movements of cell populations are generally accompanied by local changes in the shapes of individual cells. Several authors have attempted to correlate observed cell shape changes to the morphogenetic process in which they participate; these workers have occupied themselves primarily with tracing and cataloging the patterns of cell movement via lineage and "fate-map" studies. These studies, while necessary to understanding morphogenetic patterns, do not suffice to *explain* the patterns. This is because they are "kinematic" descriptions only, i.e., movements of cells are recorded, but the forces which drive the movements are not addressed. In recent years there have been great improvements in our understanding of the mechanisms for generating the forces responsible for cell shape change. We now know that cytoplasm contains a structural meshwork (cytoskeleton) composed of protein fibers (microtubules, actin filaments, and intermediate filaments), and that these fibers, collaborating in various combinations, can sustain both tensile and compressive stresses and can transduce chemical energy to active force generation (cf. Clark and Spudich, 1976; Korn, 1978; Snyder and McIntosh, 1976). Thus, the presumed machinery for driving cell shape change is beginning to be understood. Although precise details of the molecular mechanisms underlying the action of the cytoskeleton are far from clear, we believe that enough is known for us to draw on these cellular mechanisms as we proceed to the next level of description. We address ourselves here to the problem of how local cell shape changes are orchestrated into global morphogenetic movements of cell populations in embryonic epithelia.

2. THE BASIC MODEL

2.1. Hypotheses

We will present the model in the form of a set of hypotheses and discuss the consequences in a descriptive, qualitative fashion. Evidence in support of the hypotheses will then be presented. We reserve the quantitative formulation of the model for the appendices.

Consider first a single layer of uniform-sized cells, as shown in Fig. 1. These cells are attached to one another at their apical periphery so that the integrity of the external surface is maintained. For now we will also

[1] To whom correspondence should be addressed at Department of Mathematical Sciences, Rensselaer Polytechnic Institute, Troy, N. Y. 12181.

0012-1606/81/100446-17$02.00/0

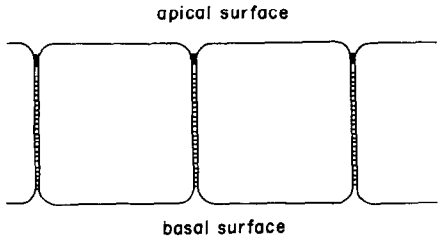

FIG. 1. Schematic of an epithelial cell layer in cross section showing apical junctions.

insist that the cells adhere to one another laterally; one can also allow lateral slippage between cells. The mechanical properties of the cells are the crucial feature of the model, which we now state in the form of hypotheses.

(a) Beneath the apical surface, each cell contains a network of contractile fibers (microfilaments) which are anchored to the plasma membrane at the lateral periphery of the cell (e.g., the zonula adherens, cf. Spooner, (1975)). This is shown schematically in Fig. 2a. For the purposes of the model, we need not specify the precise configuration of these elements; we specify only that their contraction shortens the apical circumference of the cell and reduces the apical surface area (cf. Fig. 2b). Thus, a cell can deform to a trapezoidal cross section as a result of the "purse-string" contraction occurring in the apical cortex. Whether or not apical constriction actually occurs depends on whether the contractile filaments generate forces large enough to overcome internal viscous forces and tractions applied externally by neighboring cells.

(b) We shall assume that, during the contraction process, the volume of each cell remains essentially constant. Thus, the constant volume constraint will induce the cell to elongate basally in response to an apical contraction. We postpone specifying how the contractile fibers and structural reinforcing microtubules are distributed elsewhere in the cell. We suppose only that their distribution leads to cell boundaries that act like passive viscoelastic structures, and bulk interior cytoplasm that acts like a passive viscoelastic solid (cf. Marsland, 1956; Taylor and Condelis, 1979).

(c) The apical contractile filaments constitute an active (i.e., excitable) system as follows. (i) If an apical fiber is stretched a *small* amount, by the drawing apart of the apical surface, it acts as an elastic material and when released; contracts back to its original length. (ii) If, however, the apical bundle is stretched beyond a certain point, the contractile system "fires" and an active contraction is triggered. This "rapid" contractions works to shrink the apical bundle as shown in Fig. 2b. The system does not return to its original configuration; instead, it remains "frozen" in a new, contracted state with an apical surface area smaller than before.

The viscoelastic properties of the apical filament bundle implied by hypothesis (c) are summarized in Fig. 3. The mathematical model underlying Fig. 3 is given in Appendix 1.

2.2. Description of Mechanical Properties

The description of the mechanical properties of the microfilament bundle described in Fig. 3 can be schematized as the mechanical model shown in Fig. 4. The internal viscoelastic properties of the apical bundle are represented by a dashpot with viscosity μ, and a spring of elasticity k. The elastic restoring force of the spring is a function of the difference between the actual and rest lengths,

$$F_{\text{elas}} = -k(L - L_0), \tag{1}$$

while the viscous drag force is proportional to the velocity of contraction,

$$F_{\text{visc}} = -\mu \frac{dL}{dt}. \tag{2}$$

The motion of this mechanical system must obey Newton's laws:

$$\text{mass} \times \text{acceleration} = \text{sum of forces}.$$

That is,

$$m \frac{d^2L}{dt^2} = F_{\text{elas}} + F_{\text{visc}} + F_{\text{load}}, \tag{3}$$

where F_{load} is the force exerted on the bundle, parallel to the bundle by neighboring systems, and m represents the net mass moved by a length change of the band.

A simple argument, sketched in Appendix 2, demonstrates the following crucial fact. For virtually all embryological processes we can completely neglect the effects of inertial forces. That is, if we compare the magnitude of the acceleration term with the viscous term by using the dimensionless ratio

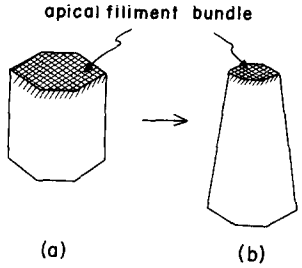

FIG. 2. (a) Network of contractile filaments in the apical region of an epithelial cell. (b) "Purse-string" contraction of the apical circumference by the apical bundle.

$$R = \left[m \frac{d^2L}{dt^2} \Big/ \mu \frac{dL}{dt} \right], \quad (4)$$

we find that $R < 10^{-5}$. Therefore, the motion of the filament bundle model is always such that viscous forces exactly balance elastic and external loading forces. Thus the equation describing the system is (3) with its left-hand side set to zero and Eqs. (1) and (2) substituted. This can be written as

$$\frac{dL}{dt} = -\frac{k}{\mu}(L - L_0) + \frac{1}{\mu} F_{\text{load}}. \quad (5)$$

That inertial forces are not a factor in morphogenetic processes is a crucial and little appreciated fact, and leads to some surprising and counterintuitive phenomena which will be discussed below.

To complete the description of the model we need to describe how the rest length, L_0, varies. This can be defined by a differential equation specifying how L_0 varies in time when the spring is stretched:

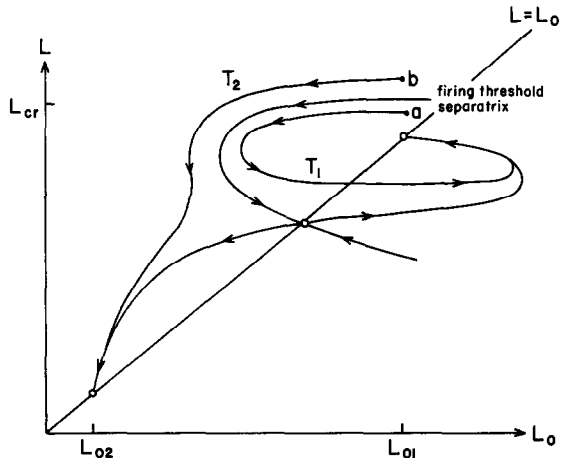

FIG. 3. Our postulates concerning the viscoelastic properties of the apical circumferential bundle of contractile filaments. The vertical axis (L) represents the actual instantaneous length of the cell's apical bundle. The horizontal axis (L_0) represents the equilibrium (rest) length of the bundle; i.e., the length it would assume in the absence of stretching forces. The apical bundle is stress-free only when the actual length equals the equilibrium length: $L = L_0$. In the simplest case, we shall assume that the apical bundle has only two stable equilibrium lengths: long (L_{01}) and short (L_{02}). By stable, we mean that following a small displacement in the actual length (L), the system returns to the same equilibrium point. For example, a dilation of the fiber bundle length from L_{01} to a point a, returns to L_{01} along a trajectory, T_1. Separating the two stable equilibria is a "firing threshold." A dilation from L_{01} to a point b which exceeds the firing threshold will not return to L_{01}, but will contract along a trajectory T_2 to the shorter equilibrium length L_{02}. It is important to note that the trajectories traced out in (L_0, L) space describe the visoelastic response of an isolated bundle of contractile filaments, i.e., one experiencing no resisting forces other than those generated internally by their own deformation.

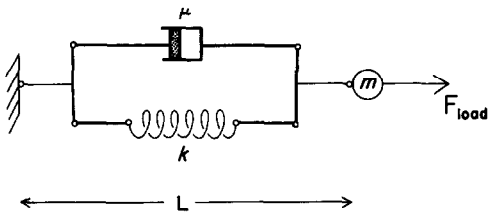

FIG. 4. Schematic of viscoelastic unit used to model a filament bundle.

$$\frac{dL_0}{dt} = G(L, L_0). \quad (6)$$

The exact form of the function $G(L,L_0)$ used in our calculations is given in Appendix 1; however, the results depend only on its qualitative features.

Equations (5) and (6) describe the dynamic behavior of a single apical filament bundle. Figure 3 describes the qualitative features of the fiber behavior for the case where the neighbor forces, (F_{load}), vanish.

2.3. Construction of Mechanical Model

The next step is to construct a mechanical model of a cell using the viscoelastic filament model. We do this as follows. Figure 5 shows a cross section of a typical cuboidal epithelial cell. Each face of the cell is represented by one of the viscoelastic elements described above. For most of the applications we shall address, only the apical element need be active.

The diagonal elements are required to model the internal viscoelastic properties of the cell's microtubular cytoskeleton. Finally, we shall assume that however the cell changes its shape, the internal volume remains constant (cf. Appendix 3).

If the apical surface of the cell is stretched beyond the firing threshold, then the cell will undergo a cycle of shape change, as shown in Fig. 6. The shape history of each cell is computed by solving a collection of dif-

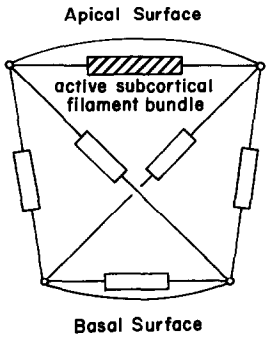

FIG. 5. Cross section of an epithelial cell showing the arrangement of viscelastic units modeling the cytoskeleton. In our model, only the apical region is mechanically excitable.

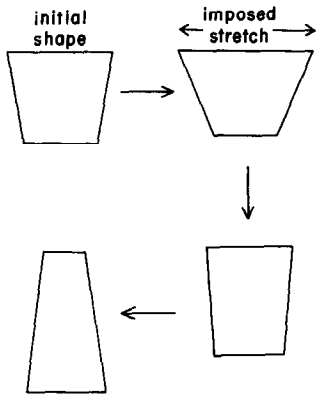

FIG. 6. The sequence of shapes assumed by a cell following a supercritical dilation of the apical filament bundle.

ferential equations like (5) and (6), describing each viscoelastic element. In the next section we shall examine the dynamical behavior of assemblies of such cells. By varying the geometrical and mechanical parameters of the viscoelastic elements we will be able to mimic the time course of a number of interesting epithelial motions.

3. APPLICATIONS OF THE MODEL

In this section we shall demonstrate how large-scale epithelial motions can be coordinated by mechanical action alone. Initially, we shall restrict ourselves to simple geometric configurations (i.e., spheres and cylinders) and to situations where cells do not change neighbors. These restrictions will be lifted in subsequent publications.

3.1. Gastrulation

The simplest epithelial arrangement is a spherical monolayer of uniform-sized cells whose apical peripheries are firmly attached. This closely approximates the configuration of blastomeres in amphioxus (Conklin, 1932) and sea urchins (Gustafson and Wolpert, 1967). Since the blastula is approximately rotationally summetric we can reduce the calculation considerably by examining a longitudinal cross section. Therefore, consider the cross-sectional ring of cells shown in Fig. 7a. If one of the cells "fires" and undergoes a rapid apical contraction, the following sequence of events occurs (refer to Fig. 7). The trigger cell in contracting its apical surface dilates the apical surface of its neighbors. If this dilation is sufficiently large, the neighboring cells will "fire" and undergo a rapid apical contraction as well. Thus the contraction of the trigger cell can initiate a spreading wave of contraction as each cell stretches its neighbors' surfaces causing them to commence their contraction cycle. We therefore predict that the apical surface of the blastula constitutes an "excitable," or "active," medium which can propagate contraction waves in a manner analogous to the propagation of depolarization waves along nerve axons (cf. Hodgkin and Huxley, 1952) and the propagation of electrical waves over the brain's cortical surface (cf. Cowan, 1970).

The significance of contraction waves lies in the fact that a spreading wave can generate an invagination in the cell layer. This is shown in the sequence shown in Fig. 7 which is taken from a computer-generated movie obtained by solving the model equations sequentially in time. The mathematical details of the model used to generate Fig. 7 are described in Appendix 4. The invagination occurs roughly as follows. The contraction of the trigger cell and its neighbors initiates a "dimple" in the cell layer. As the wave spreads radially from the nucleation center the cell layer buckles inward at the wavefront, so that the outgoing contraction wave is converted into a buckling wave. The buckling in effect "pumps" cells into the interior of the sphere converting a convex surface into a concave one.

The velocity of the buckling wave and the extent of the invagination depends on several features of the cells' mechanical constitution: (a) the viscoelastic properties of the fiber bundle, i.e., the velocity and strength of the contraction cycle, the firing threshold, and the elastic response to subthreshold excitation; (b) the viscous resistance of the cell to dilations and contractions; (c) the mechanical properties of the cell-to-cell junctions; e.g., viscous sliding of lateral surfaces may change the invagination pattern; (d) in addition to the above hypotheses concerning the mechanical constitution of each cell, a model of gastrulation requires specifying how the (incompressible) fluid filling the blastocoel is forced out during gastrulation. This is described in Appendix 4. Roughly, we assume that the blastocoel fluid is passively extruded out when the interior hydrostatic pressure is elevated above ambient (external) pressure by circumferential tension in the cell sheet.

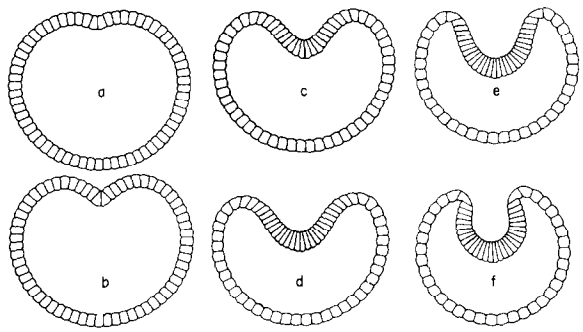

FIG. 7. Computer simulation of gastrulation in sea urchin. The frames (ordered, a, b, c, . . . , f), were extracted from a computer-generated film obtained by solving the model's equations derived in Appendix 4.

Our model does not specify the mechanism for triggering the contraction of the first cell—we take it as an initial condition, given *a priori*. It is a common aspect of morphogenesis that, before a developmental process visibly unfolds, the stage has been set by the previous processes. Thus, in the case of gastrulation, the information designating the site of invagination would be established in the blastula. Our model reduces the need for prepattern to specifying only the site of initiation and the distribution of contractile machinery in the cells. It eliminates a need for clocks or programs in the other cells participating in invagination.

Several possible mechanisms for terminating invagination may be envisioned. Invagination may cease when the two cell layers abutt one another, so that cessation of gastrulation may result simply from mechanical obstruction. Alternatively, the buckling wave may run out of active cells. A particularly obvious mechanism of termination is illustrated by *Volvox carteri* (Kelland, 1977; Viamontes and Kirk, 1977). In this organism, the spherical integrity of the "blastula" is pierced by an opening (the phialopore). A bending wave, beginning at the lip of the phialopore, propagates all the way to the opposite pole, thereby turning the spherical colony inside out.

Whatever the mechanism of initiation and termination, the crucial aspect of our model is that, once triggered, the morphogenetic process of invagination proceeds on its own, directed solely by the global balance of mechanical forces generated locally by each cell, and with no requirement for individually preprogrammed sequences or patterns of cell shape change.

3.2. The Ventral Furrow of Drosophila

In addition to simple invagination, epithelial sheets can roll themselves into tubes. Figure 8 models a cross section of a *Drosophila blastula* showing the ventral furrow (Turner and Mahowald, 1977). To simulate this morphogenetic process we take advantage of the embryo's cylindrical symmetry and model only a cross section as before. Figure 8 is a sequence extracted from a computer-drawn movie of this process as generated by the model. Aside from changing the number and size of the cells to conform more with the actual geometry, a number of other parameters was altered. In particular, the cavity enclosed by the epithelial sheet was maintained at a constant volume to represent a leakproof yolk-filled interior, in contrast to the leaky blastocoel in the gastrulation simulation.

3.3. Neurulation in amphibians

In amphibians (and in amphioxus), the formation of the neural plate and the neural tube comes about by a remodeling of the neural ectoderm. This process is accompanied by changes in the shape of the cells constituting the neural ectoderm, and it appears likely that the coordinated shape changes of the individual cells constitutes the driving force behind neurulation (Burnside, 1973). Jacobson and Gordon (1976) constructed a computer simulation of the formation of the neural plate based on different autonomous, preprogrammed schedules of shape changes for different regions of the neural ectoderm. Their simulations did not address the folding of the neural tube, however. In our model we can achieve characteristic neural plate formation and folding by lowering the firing threshold in the active cells constituting the presumptive neural plate. Figure 9 is a sequence extracted from another computer movie. The dynamics of this folding is quite different from that of the ventral furrow. The contraction of the first few cells is transmitted "instantaneously" to the rest of the cells which, because of their lowered threshold, fire quickly and adjust their *rest* lengths, L_0, to near their final values. Thus, before the actual deformation

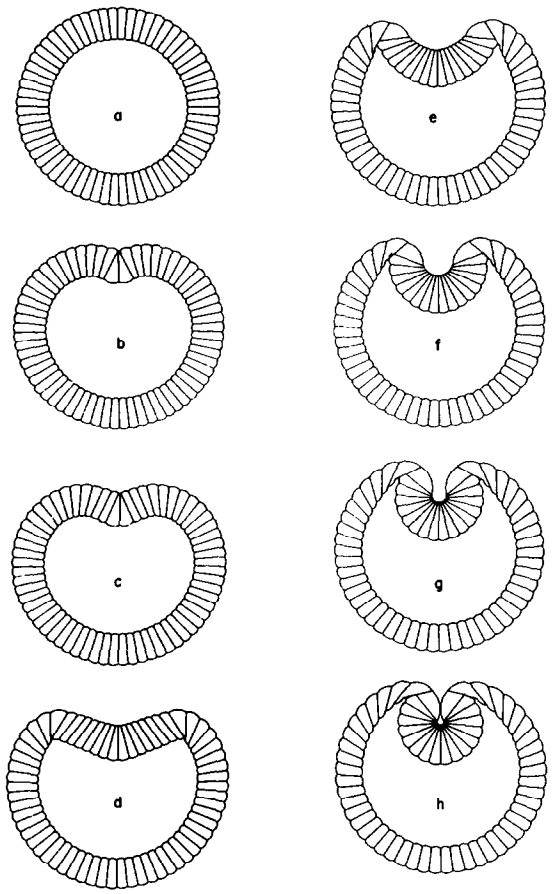

FIG. 8. Computer simulation of ventral furrow formation in *Drosophila*.

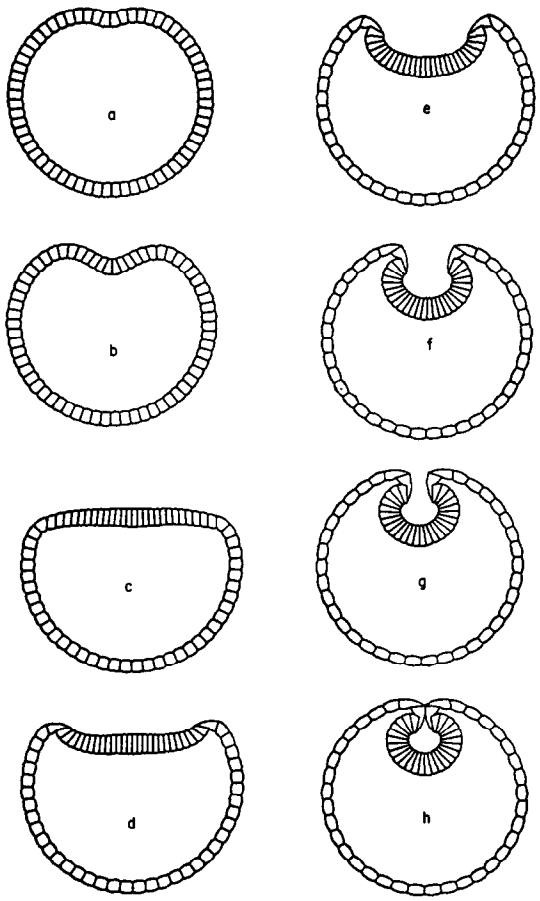

FIG. 9. Computer simulation of neural tube formation in amphibians.

proceeds very far, all of the active cells have been mechanically "set"; in a sense the "prepattern" for contraction is established by mechanical signalling before the time of neural plate flattening. Thus, this "plate" structure (Fig. 9c), even were it isolated from the rest of the cells, would nevertheless proceed to roll into a tube. Indeed, excised neural ectoderm at the plate stage will fold "as if" the cell shrinkage pattern already had been specified. In this situation, the apparent simultaneity of response by participating cells (on the time scale of the tissue movements) is a consequence of the low Reynolds number regime, and there is no need to invoke cellular clocks as coordinating mechanisms.

The neuralation model differs in an important respect from the gastrulation and ventral furrow simulations. In the latter two cases we could invoke spherical and cylindrical symmetry, respectively, to justify treating only a cross section of the tissue. This is not the case in neurulation, however. Burnside (1973) has mapped the trajectories of cells in the neural ectoderm and found that there are major axial (anterior-posterior) as well as transversal movements which accompany neural plate formation. Moreover, Jacobson and Gordon (1976) have shown that the cells of the supranotochordal region must repack longitudinally in order for the neural plate to achieve its characteristic keyhole shape. Therefore in the simulation of Fig. 9 cells are flowing through plane of the cross section, so that the "cells" shown in successive frames of the sequence may represent different cells: the cells which happen to be in that plane at that time. The simulation, thus, does not keep track of actual cells, but does account for the circumferential forces which produce folding. A complete study of neural plate formation and folding which includes the effects of cell rearrangement (cf. Section 3.4.E) is in preparation (Jacobson *et al.*, to appear).

3.4. Other Applications of the Model

The mechanical model developed above is capable of generating a number of geometrical structures other than buckling and invagination, depending on the geometric configuration of the cells, their viscoelastic parameters and how the contractile machinery is distributed within the cell. Below we briefly describe some of these configurations; a more complete discussion will be presented elsewhere.

(A) Evagination and exogastrulation. As certain of the elastic parameters are varied a bifurcation occurs such that propagating apical contraction wave buckles the cell layer outward producing an evagination. Figure 10 shows an example.

(B) Epithelial thickening. Instead of propagating a buckling wave the cell layer can simply thicken up (placode formation) as in the neural plate simulation, each cell passing from a cuboidal to a columnar configuration. Because mechanical forces are "effectively" long range, this thickening up may appear almost simultaneously over the sheet giving the appearance that each cell is independently programmed.

Interestingly, it is possible to generate a stationary almost-periodic pattern of thick and thin regions analagous to that observed at the initiation of hair follicle formation (Odell *et al.*, 1981b).

(C) Contraction waves in a continuous medium. Time lapse films of the surface of amphibian blastulas approaching gastrulation show that the blastula surface is frequently swept by undulating deformation waves which appear to spread outward from an initial focus. These dimples have the appearance of the initial stages of gastrulation; however, their amplitude is considerably smaller. Similarly, some fertilized eggs which have been treated so as to suppress cleavage, nevertheless,

at the appropriate time initiate (but do not continue) surface invagination that resembles that of gastrulation (Holtfreter, 1943). This process, called pseudogastrulation, strongly suggests that the cortical surface of the egg is also mechanically active and can support wave propagation. Indeed, Marc Kirschner (personal communication) has filmed a striking phenomenon: just preceding each cleavage, up until quite late in blastulation, a wave of contraction sweeps out from the presumptive cleavage origin over the egg surface.

These observations suggest that the mechanical capacity for contraction waves and invagination is present in the cortical layer quite early in development, and that the subsequent subdivision of the cytoplasm via cleavage is not really an essential feature of the contraction wave mechanism. The model, as we have developed it, is cellular; however, by passing to the limit of infinitesimal cell size, a continuum version of the model can be constructed. The properties of this limiting model—especially its ability to support buckling waves—is presently under investigation.

(D) Epithelial folding in other tissue systems. Epithelial folding in gastrulation, such as we have described here, resembles, in many respects, epithelial folding observed in other tissues later in development (for example, lens, optic vescicle, and nasal placode) (cf. Spooner, 1975). Moreover, Bernfield and Barerjee (1978) has reported observing wave-like contractions accompanying formation of salivary glands. It is tempting to speculate that (evolution being conservative) the same mechanism is common to all such phenomena.

(E) Repacking of epithelial cells. In addition folding and invagination, epithelial layers are capable of rearranging their configuration by repacking the constituent cells. This process involves more or less systematic cell neighbor exchanges and probably acts in concert with differential adhesion between cell types. For example, the proper shaping of the neural plate depends on repacking of the supranotochordal region (Jacobson and Gordon, 1976). Also, Fristrom (Fristrom and Fristrom, 1975; Fristrom and Chihara, 1978) has shown that the evagination of *Drosophila* imaginal discs depends largely on the repacking and realignment of the epithelial cells. By modifying our model to allow for cell slippage driven by contraction spasms of the participating cells, we can model these processes as well. This will be treated fully in a subsequent publication.

4. CHEMICAL SIGNALING

In our description of the model we have eschewed any mention of chemical signaling between cells; mechanical deformations alone trigger the contraction cycles. However, Fig. 3 is a purely phenomenological description of the contractile mechanism; there is, in principle, no difficulty in incorporating chemical signaling mechanisms as well. For example, the "firing" of the apical contractile machinery is almost certainly initiated by the release of sequestered Ca^{2+}, or its influx from external sources (cf. Hitchcock, 1977). Moreover, it is known that epithelial cells can communicate small ions and molecules, via gap junctions. Thus it is possible that the proximal stimulus which actually triggers a cell contraction may be flux of ions or molecules through such junctions from a neighboring cell which has already contracted, rather than the direct mechanical action of stretching the cell cortex. If this were in fact the mechanism for triggering contraction, then the action of the "morphogen" would be "local." It is relatively straightforward to modify the model so as to include such a local, cell-to-cell, signaling mechanism, and this will be treated in detail in a subsequent publication (Odell *et al.*, 1981a).

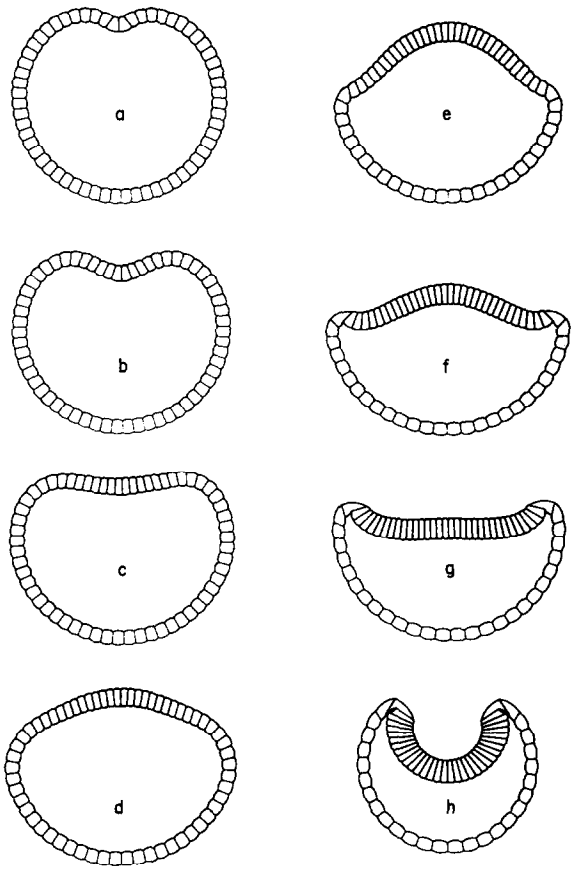

FIG. 10. Computer simulation of exogastrulation. See Appendix 4 for a listing of parameter values used in the simulations in Figs. 7-10.

5. EXPERIMENTAL EVIDENCE IN SUPPORT OF THE MODEL

5.1. Apical Contractile Machinery

Apical filament bands contract quite slowly. Frame-by-frame analysis of time lapse films (made and kindly

supplied by Dr. Anton Jacobson) of spasmodic contraction waves, propagating over the surface of a stage 8 *Taricha tarosa* blastula, reveals that the apical circumference contracts by a factor of about 7.5 in 19 min. In these large cells, the contraction velocity peaked at about 12 μm/min for a band that contracted from 113 to 15 μm. This relatively slow contraction time must be kept in mind while considering contractile protein systems as candidates for the force generation machinery driving morphogenetic movements.

That embryonic epithelial cells have a contractile gel layer beneath their apical surfaces has long been postulated by developmental biologists to explain numerous aspects of epithelial behavior (cf. Waddington, 1940; Holtfreter, 1943; Lewis, 1947). Definitive ultrastructural characterization of this contractile layer was first provided by Baker and Schroeder (1967), who showed that the apical ends from neural plate cells possess a purse-string like an arrangement of 60-Å-diameter microfilaments. Similar filament arrangements have been reported in numerous other embryonic epithelia (cf. Spooner, 1975).

It is now generally accepted that 60-Å-diameter microfilaments are actin filaments (cf. Korn, 1978). This conclusion is based on the ubiquitous occurrence of actin in cells and on histochemical procedures (heavy neuromyosin or subfragment decoration) which demonstrate *in situ* that filaments are composed of actin. In several embryonic epithelia, myosin-fragment decoration procedures have shown that the apical microfilaments are actin. Though myosin thick filaments are rarely observed in nonmuscle cells, it has now been shown biochemically that virtually all cells do contain myosin (cf. Korn, 1978). Thus, the contractile machinery responsible for force development in muscle is present in embryonic epithelial cells. In addition, filament arrangements appropriate to produce a purse-string-like contraction of the cell apex have been observed (Baker and Schroeder, 1967; Burnside, 1973).

5.2. Stretch as a Trigger for Contraction

Precedent for this aspect of the model comes from the stretch activation of unitary smooth muscles (cf. Axelsson, 1971; Prosser, 1974) and insect flight muscle (Wray, 1979). In smooth muscles, stretch at a critical velocity depolarizes the cell and initiates repetitive spikes; these membrane changes produce calcium influx (and release from internal stores) and thus initiate contraction (Prosser, 1974). Slow stretch may fail to initiate spikes because the membrane accommodates (Axelsson, 1971). Similar stretch-induced alterations in membrane potential and conductance could control calcium release in embryonic epithelial cells, and thus provide the mode of propagating the contraction event from cell to cell. Initiation of spikes would not be a necessary aspect of the induction; changes in potential could suffice.

The threshold for triggering contraction assumed in the model might, for example, resemble that for speed of stretch in triggering smooth muscle contraction. It would be possible to design a model similar to ours, in which degree of contraction is proportional to prestretch. Such a model would invaginate and produce shape change in a similar manner.

A cellular basis for the shape changes of the model might be envisioned based on alternative states of actin filaments, either crosslinked into a stable but quiescent gel or free to interact with myosin to produce contraction (cf. Taylor and Condeelis, 1979). We assume that the apical actin filaments are crosslinked onto a viscoelastic gel when cytoplasmic calcium concentrations are low (e.g. $<10^{-6}$ *m*) (Taylor and Condeelis, 1979). This gel stabilizes the conformation of the cell apex. Stretch triggers calcium influx or release from internal stores (as a result, for example, of stretch-induced changes in membrane potential or permeability). As cytoplasmic calcium levels exceed 10^{-6} *m*, new conditions are established: (a) the crosslinkers are released from the actin filaments (thereby dissolving the gel), (b) myosin is now capable of interacting with the actin filaments to produce ATP-dependent sliding, and (c) the purse-string arrangement of filaments contracts, reducing the apex to a new and smaller diameter. We also assume that after stretch-induced release, calcium is resequestered by the cell (as occurs in muscle), so that cytoplasmic calcium levels again soon fall below 10^{-6} *m*. Thus, contraction is inactivated and the apical actin gel is reformed, now stabilizing the cell apex at a new, smaller resting diameter. This apical actin network then serves as a cytoskeleton for stabilizing the new shape and transmitting the global forces produced by contractions elsewhere.

6. RELATION TO OTHER MORPHOGENETIC MODELS

Several theories have evolved over the past several decades to "explain" the programming of morphogenetic processes in cell populations (pattern formation). How satisfying a theory is depends on how phenomenological an explanation one finds acceptable. Some theories, such as Waddington's (1940) notion of an "epigenetic landscape" are basically allegories, i.e., mechanical analogies which appear almost impervious to experimental disproof.

Lewis (1947) constructed a mechanical model, consisting of brass plates, hinged at their centers to a flexible spine, and tied, each to its neighbors, by rubber bands at the protruding ends. The plates represented

the lateral surface of cells, while rubber bands modeled tension-generating machinery at the basal and apical ends. By variously distributing rubber bands on his model, he was able to reproduce a variety of possible epithelial cell sheet foldings. This assumed the existence of some internal mechanism for timing and positioning local changes in the rubber band density along the sheets.

The most influential of the current theories of pattern formation involve the notion of "morphogen gradients" conceived by Turing (1952). The morphogens are unspecified instructional molecules which are presumed to be differentially distributed (e.g., by diffusion) over a cellular population. Pattern is established when each cell of the population then responds to the local concentration of the morphogen by assuming a particular differentiation state. Meinhart and Gierer (1974), for example, have shown that a diffusing field of "activating" and "inhibiting" morphogens can generate a variety of concentration patterns which are remarkably suggestive of observed morphogenetic patterns.

Some reservations, however, should be noted. Unfortunately, except for cyclic AMP in slime mold aggregation, very few morphogens have been identified. Moreover, each cell must be able to "read" the local concentrations of morphogens accurately and differentiate accordingly. Thus the cell pattern is but a passive reflection of a preexisting morphogen pattern. In effect, the problem of cell patterns has been replaced by the physical-chemical problem of distributing the morphogens appropriately by intercellular diffusion and reaction.

Building on this work, Gierer (1977) developed a formalism for characterizing cell sheet mechanics. He assumes that reaction and diffusion establish time-varying morphogen patterns in the cell sheet. He assigns to each cell a mechanical potential energy function whose value depends on the morphogen values and on the surface area the cell has in common with its neighboring cells and the exterior environment. The mechanical configuration of the cell sheet is computed at each time by minimizing the total potential energy. The relationship between the ad hoc potential and the forces generating the motion is not specified.

Wolpert's (1969) theory of "positional information" has been especially influential to current thinking about morphogenetic processes as disparate as chondrogenesis (Summerbell *et al.*, 1973) somitogenesis (Cooke and Zeeman, 1976), regeneration (Goodwin and Cohen, 1969; Bryant, *et al.*, 1977) and neurulation (Jacobson and Gordon, 1976). Unfortunately, the mechanisms proposed by which a cell "knows" its position usually depend on morphogen gradients, clonal lines, or are left unspecified. For example, in an elegant study of neurulation, Jacobson and Gordon (1976) were able to reproduce, on a computer, the observed patterns of cell shape change and movement which accompany the forming of the neural plate. To do this, however, they had to assign to each cell an autonomous program of shape change as well as a cellular "clock" to time and synchronize the cell population.

Viamontes *et al.* (1980) have analyzed and modeled mathematically the inversion of *Volvox carteri* embryos. They have measured spatiotemporal patterns of shape change exhibited by participating cells and have correlated these local shape changes with global deformations of the embryonic colony. Their mathematical model is kinematic only (that is, they impose prescheduled shape changes rather than deducing shape changes from cell-generated forces), and they do not address the question of how the cells coordinate their activities. Nevertheless, they give the most compelling argument we know of that the global (inversion) deformation of the cell sheet is caused by local shape changes of individual cells (and by active radial translocation of the cytoplasmic bridges between cells), and that these changes are caused by forces generated autonomously by each cell using its microtubule and microfilament force transduction machinery. In addition, this paper contains observations (see the discussion of "elastic snap through") indicating that the composite elasticity and viscosity of embryonic epithelial cells are such as to yield an elastoviscous relaxation time of $\sim 5 \text{ min} = \mu/k$.

In this study we want to minimize both the number of complex instructions (e.g., morphogens and clocks) as well as the genetic programming required to generate morphogenetic patterns. It is, of course, conceivable that each individual cell in the blastula is genetically programmed to execute a sequence of instructions directing each movement that cell performs as well as its precise timing. However, we regard such a view as evolutionarily implausible. Therefore, we have constrained ourselves by two considerations. First, since the aspect of morphogenesis we are addressing is the geometrical shaping of cell populations, we wanted to ascertain whether a global morphogenetic process, such as gastrulation, could be programmed by purely mechanical effects, without introducing prepatterns of chemical or electrical signals. Second, we wanted to minimize the load of genetic preprogramming required to generate morphogenetic patterns. We felt that to equip each cell with an autonomous program, and a precise "clock" for activating that program, was unesthetic and probably unnecessary. At least part of the burden of pattern formation and regulation may be taken up by the equilibration of purely mechanical forces.

Our model, therefore, is built on Newton's laws of motion and consists of a dynamical system of ordinary differential equations whose solution determines the global time history of the cell sheet geometry, given its initial configuration. Thus our "explanation" of how epithelial morphogenesis proceeds rests on solving the mechanical equations of motion based on the balance of cell-generated forces. That is, we view cell forces, not clocks, morphogens, or potentials, as the "cause" which "explains" the morphogenetic motion. We hope that the logical extension of this model will be to generate a series of hypotheses on the molecular basis for reorganization of contractile proteins inside the cell which would explain the phenomenological rules defined in this paper.

CONCLUSION

The deformations of cells that shape the embryo arise from forces generated by participating cells. The problem of morphogenesis is to determine how these local forces are generated and coordinated so as to create organized multicellular structures. We have proposed one such mechanism for coordinating epithelial cell populations which can produce a variety of geometrical configurations, including folding and invagination. In our model, coordination at the population level arises from the local behavior of each cell automatically; there is no need to introduce poorly understood devices such as morphogens and cellular clocks.

We have based our theory solely on two assumptions: first that during morphogenetic movements, epithelial cell populations obey the laws of conservation of mass and momentum, and second, that each cell acts as an excitable element in the sense described above. The first of these assumptions is hardly disputable. The second assumption is a plausible hypothesis on how contractile proteins change the shapes of cells. That they do is now well established despite the fact that the molecular mechanisms are still not completely understood.

The coordination of epithelial cell shape changes is accompanied, we hypothesize, by the propagation of mechanical contraction waves. Each cell is equipped with subcortical contractile fibers (e.g., microfilaments) which can deform the shape of the cell. These fibers are organized so as to constitute an "excitable" viscoelastic medium in the following sense. Small dilations in cell shape are resisted by simple elastic restoring forces. Sufficiently large dilations, however, trigger larger restoring forces which, if not resisted externally, cause the fibers to contract beyond their original equilibrium configuration in a fashion analogous to smooth muscle action. If the contraction of each cell deforms its neighbors sufficiently, a wave of cell shape change can be propagated across an epithelial layer. Depending on how the contractile machinery is distributed within the cells a variety of dynamic and static configurations can be generated: invaginations, exvaginations, uniform and periodic thickenings, wave propagation, and tube formation.

APPENDIX 1: MATHEMATICAL MODEL OF AN ISOLATED APICAL FILAMENT BUNDLE

The two dynamical variables characterizing the state of a single apical filament bundle at time t are its actual length, $L(t)$, and its rest length, $L_0(t)$. When the filament is isolated, suffering no externally applied forces, the dynamical behavior of these two variables is governed by eqs. (5) (Newton's second law, with $F_{\text{load}} = 0$) and (6):

$$\frac{dL}{dt} = -\frac{k(\cdot)}{\mu}[L - L_0], \tag{A1.1}$$

$$\frac{dL_0}{dt} = G(L, L_0). \tag{A1.2}$$

When G is zero, the filament band is a passive viscously damped spring. When G is chosen appropriately, the spring becomes active and mechanically triggerable. Figure 3 consists of selected trajectories from a phase plane portrait of the second-order autonomous ordinary differential equation system (A1.1) and (A1.2). We propose here one concrete choice (among infinitely many possible choices) of the function G that will yield a phase portrait similar to the one shown in Fig. 3.

We make this concrete selection of the functional form of G not because we believe it alone to be correct, but because we cannot implement a numerical simulation without having a numerically calculable right-hand side of Eq. (A1.2). Having actually run simulations using several different choices of $G(L, L_0)$, we are certain that the detailed functional form of G is unimportant, provided only that it generates the kind of phase portrait sketched in Fig. 3. Thus, in this first paper, we parameterize the functional recipe for G in such a way that changes in its parameters correspond simply and directly to known deformations of the phase portrait. Such a recipe is the following:

$$\frac{dL_0}{dt} = \gamma[\epsilon_1^2 - LL_0]\left\{\left(\frac{L-\eta}{\epsilon_3}\right)^2 + \left(\frac{L_0-\eta}{\epsilon_4}\right)^2 - 1\right\}, \tag{A1.3}$$

where

$$\eta \equiv 1 - \frac{\epsilon_3\epsilon_4}{(\epsilon_3^2 + \epsilon_4^2)^{1/2}}.$$

In (A1.1) and (A1.3) we use scaled (dimensionless) versions of L and L_0 such that the untriggered rest state of the filament band occurs at unit lengths,

$$L = L_0 = 1 \quad (= L_{01} \text{ in Fig. 3}).$$

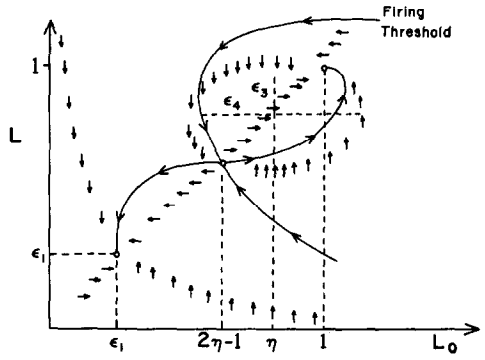

FIG. 11. Phase portrait in the (L, L_0) plane for Eqs. (A1.1) and (A1.3) showing how the parameters ϵ_1, ϵ_3, ϵ_4 control the location of the nullclines (depicted as loci of vertical and horizontal flow arrows).

This choice of G is convenient because, with it, the L_0 nullcline in the (L_0, L) phase plane (the locus where $G = 0$) consists of the hyperbola, $LL_0 = \epsilon_1^2$, where the term in square brackets vanishes, and the ellipse

$$\left(\frac{L-\eta}{\epsilon_3}\right)^2 + \left(\frac{L_0-\eta}{\epsilon_4}\right)^2 = 1$$

centered at (η, η) with axes set by ϵ_3 and ϵ_4. The L nullcline is the 45° line, $L = L_0$. Figure 11 depicts these nullclines and shows how the parameters ϵ_1, ϵ_3, and ϵ_4 determine their positions.

ϵ_1 is the fully contracted length after triggering. Increasing ϵ_3 raises the firing threshold separatrix.

We model contractile excitability of the filament bundle not only by having the rest length, L_0, decrease when a resting bundle is stretched, but also by making the spring "constant," k, increase when triggering occurs. This is done by setting

$$k(\cdot) = k_0/L_0 \tag{A1.4}$$

in (A1.1). Physically, this means that a triggered band not only wants to assume a shorter length, but also becomes stiffer than a relaxed band and pulls harder to assume it.

In a future publication (Oster *et al.*, 1981), we explain how an intracellular trigger chemical, c, whose kinetics are given by

$$\frac{dc}{dt} = \left[\begin{array}{l}\text{autocatalytic}\\ \text{production}\\ \text{of } c\end{array}\right] - \left[\begin{array}{l}\text{first-order}\\ \text{spontaneous}\\ \text{decay of } c\end{array}\right] + \left[\begin{array}{l}\text{stretch-induced}\\ \text{first-order}\\ \text{production}\\ \text{of } c\end{array}\right] \tag{A1.5}$$

and which modulates the rest length, L_0, as indicated in Fig. 12, leads to an equation for L_0 equivalent to (A1.3), and a phase portrait exactly equivalent to Fig. 3.

APPENDIX 2: INERTIAL FORCES ARE NEGLIGIBLE ON THE EMBRYONIC SCALE

The neglect of inertial forces is a central ingredient in our model, and leads to a number of important and counterintuitive effects. Below we give a brief justification of this important physical assumption. A more detailed discussion of the viscosity-dominated physics of cell motility can be found in Purcell (1977).

Consider the one-dimensional spring-dashpot unit shown in Fig. 4. Newton's equation of motion for this unit is

mass × acceleration

= sum of elastic forces and viscous forces,

$$m\frac{d^2L}{dt^2} = -k(L - L_0) - \mu\frac{dL}{dt}. \tag{A2.1}$$

In order to compare the relative magnitudes of the terms in this equation we must render them dimensionless by selecting appropriate scales for all of the variables. Using t_0 = time required for complete contraction of a filament band, $L_0(0)$ as a characteristic length, we introduce these dimensionless variables:

$$x = L/L_0 = \text{dimensionless size},$$

$$\tau = t/t_0 = \text{dimensionless time},$$

$$v_0 = L_0/t_0 = \text{dimensionless velocity}.$$

Substituting these into Eq. (A2.1) yields

$$\left[\frac{mL_0}{t_0^2}\right]\frac{d^2x}{d\tau^2} = -[kL_0](x-1) - \left[\frac{\mu L_0}{t_0}\right]\frac{dx}{d\tau} \tag{A2.2}$$

or

$$\left[\frac{mv_0}{\mu L_0}\right]\ddot{x} + \left[\frac{kL_0}{\mu v_0}\right](x-1) + \dot{x} = 0.$$

By grossly overestimating the element's volume as L_0^3, *the mass*, m, cannot be larger than ρL_0^3, where ρ is the

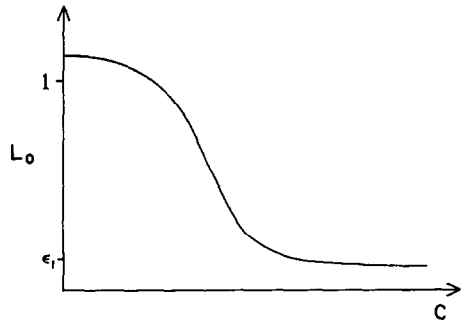

FIG. 12. The hypothesized dependence of rest length, L_0, upon trigger chemical concentration, c.

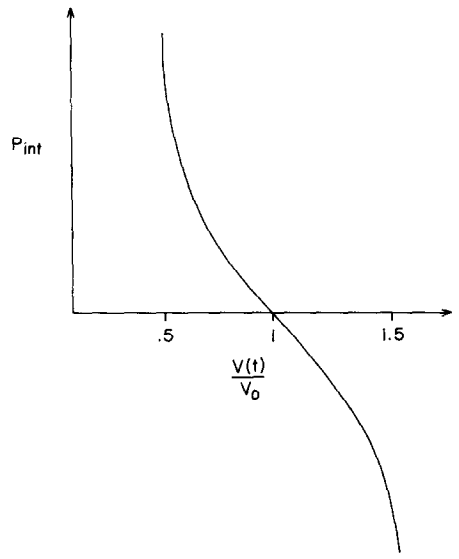

FIG. 13. The relationship between interior hydrostatic pressure, P_{int}, and the volume change, $V(t)/V_0$, of the fluid filling the cell. This is a graph of Eq. (A1.1).

density. Thus the coefficient multiplying the acceleration term is less than

$$R = \frac{\rho v_0 L_0}{\mu/L_0} = \frac{\rho v_0 L_0}{\tilde{\mu}}, \qquad \text{(A2.3)}$$

where $\tilde{\mu} = \mu/L_0$ is the liquid viscosity (i.e., the dashpot constant is actually the viscosity per unit length). Conservative estimates for these parameters are as follows. For a blastula $L_0 \sim 10^{-1}$ cm in size, embryonic movements proceed at velocities less than $v_0 = 10^{-6}$ cm/sec (i.e., $t_0 > 10^3$ sec). Cytoplasmic viscosities are far in excess of water, but to be conservative we will use the value for water: $\tilde{\mu}/\rho \sim 10^{-2}$cm/sec (actual cytoplasmic viscosities may be as high as 10^7 P!). Even with these generous estimates, $R = (10^{-6})(10^{-1})/(10^{-2}) = 10^{-5}$. Thus the inertial forces are at least 100,000 times smaller than viscous forces and we are justified in neglecting accelerations on the embryonic scale.

APPENDIX 3: THE MATHEMATICAL MODEL OF A SINGLE CELL WHOSE APICAL END IS EXCITABLE

As illustrated in Fig. 5, we model a single cell (in two-dimensional cross section) as a quadrilateral, each of whose sides, and whose diagonals,[2] are viscoelastic elements as described by Eq. (5). For the simulations presented in this paper, only the apical end of each cell is taken to be an active mechanically excitable filament band (whose behavior is modeled in Appendix 1). For other applications, any or all elements of the cell can easily be made active, with an insignificant increase in the computational complexity of the equations we present below.

To generate the differential equations that describe the motion of a single cell, we require that, at each of the cell's four corners, the sums of all forces, and of all moments, acting there be zero. This produces four vector equations that are equivalent to a system of eight scalar nonlinear first-order differential equations in implicit form. To these eight, we add one more differential equation that determines the way the excitable rest length of the apical end changes. The derivation of these equations is the subject of this appendix.

While a cell deforms in response to external loading and internal active force generation (by the apical band), we want to constrain it to maintain its original volume.[3] Exact implementation of this constraint is mathematically difficult. We have chosen to implement it only approximately as described below. Our method has the advantages (over the use of Lagrange multipliers) of mathematical simplicity and of addressing directly exactly which force mechanisms act to enforce the constraint.

We suppose the cell to be filled with a fluid that is slightly compressible. Relatively slight reductions in the volume of the quadrilateral cell cause relatively great increases in the interior hydrostatic pressure. This increased pressure, pushing out normally on all four sides, acts to inhibit volume shrinkage. The basal and apical ends of epithelial cells are not planar, but can bulge outward, as indicated schematically by curved ends in Fig. 5. We think of any reduction in the volume of our quadrilateral cell as taken up by the convex bulging of the ends, driven by increased interior hydrostatic pressure.

Let V_0 be the original volume of our cell, and $V(t)$ be its volume at time t. We assert a relationship between the interior hydrostatic pressure, P_{int}, and $V(t)/V_0$ of the sort graphed in Fig. 13. The exact recipe for this function is not important. The one we use is

$$P_{int} = \Gamma \frac{1 - R}{[(R - (1/2)][(3/2) - R)]}, \qquad \text{(A3.1)}$$

where $R \equiv V(t)/V_0$. Γ can be made arbitrarily large to keep volume changes arbitrarily small.

We now write down the force balance conditions. Figure 14 is Fig. 5 embellished with labeled quantities that keep track of the cell's cross-sectional geometry.

[2] Mechanically substantial diagonal struts are not absolutely essential. They are included to avoid a pathology that could, but rarely would, show up in the equations during simulations. Namely, without diagonal struts, a cell that assumes an exactly rectangular configuration offers no resistive force to shear.

[3] In later publications we will allow cells to actively change their volumes, by osmotic takeup of external fluid, for example, as seems to occur during gastrulation (see Conklin, 1932).

$\mathbf{x}_i$ is the (vector) position of the ith corner (node) of the cell, for $i = 1, 2, 3, 4$. The directed line element from node $\mathbf{x}_i$ to $\mathbf{x}_j$, to be thought of as a strut element of the cytoskeleton/cortical filament mesh, has associated with it:

(i) the unit vector $\mathbf{e}_{ij} = (\mathbf{x}_j - \mathbf{x}_i)/L_{ij}$ along it,

(ii) the unit outward normal vector to it, $\mathbf{n}_{ij}$ (not applicable for diagonals),

(iii) its actual length, $L_{ij} = [(\mathbf{x}_i - \mathbf{x}_j)(\mathbf{x}_i - \mathbf{x}_j)]^{1/2}$,

(iv) its rest length, $L_{0_{ij}}$,

(v) its elastic modulus function, $k_{ij} = (k_{0_{ij}}/L_{0_{ij}})$, and its viscosity, μ_{ij},

(vi) the tension in it [see Eqs. (1) and (2)].

$$T_{ij} = -k_{ij}(L_{ij} - L_{0_{ij}}) - \mu_{ij}(d/dt)L_{ij}. \qquad \text{(A3.2)}$$

An externally applied force, $\mathbf{F}_i$, acts at the node $\mathbf{x}_i$, for $i = 1, 2, 3, 4$. Since we are considering only problems in which inertial effects are negligible (see Appendix 2), the single cell can be in mechanical equilibrium only if these external forces add to zero, and generate no net moment, so we assume

$$\sum_{i=1}^{4} \mathbf{F}_i = 0, \qquad \text{(A3.3)}$$

and

$$\sum_{i=1}^{4} \mathbf{x}_i \wedge \mathbf{F}_i = 0, \qquad \text{(A3.4)}$$

where $\wedge$ denotes the vector cross product. In Appendix 4, where we discuss the equations for a ring of cells, each identical to the single cell discussed here, these forces will be those exerted by neighboring cells. Thus, $\mathbf{F}_1$ and $\mathbf{F}_2$ will represent the forces exerted by the left neighboring cell.

For now, we take the external pressure to be zero everywhere. Then the pressure force acting on an outer edge connecting $\mathbf{x}_i$ and $\mathbf{x}_j$ will be

$$(P_{\text{int}} - 0)L_{ij}\mathbf{n}_{ij}.$$

This force, distributed all along the edge, is equivalent to forces of $(1/2)(P_{\text{int}} - 0)L_{ij}\mathbf{n}_{ij}$ acting at each node, $\mathbf{x}_i$ and $\mathbf{x}_j$. (This partitioning alone achieves moment balance.)

With the above definitions and understandings, the sum of forces acting at the node $\mathbf{x}_i$, which must be zero, is

$$\mathbf{F}_i + \sum_{\substack{j=1 \\ j\neq i}}^{4} T_{ij}\mathbf{e}_{ij} + \sum_{\substack{j=1 \\ j\neq i \\ \text{(exclude diagonals)}}}^{4} (1/2)(P_{\text{int}} - 0)L_{ij}\mathbf{n}_{ij} = 0. \qquad \text{(A3.5)}$$

(A3.5) holds for $i = 1, 2, 3, 4$. $\mathbf{n}_{ij}$ is obtained by swapping the components of $\mathbf{e}_{ij}$ and changing the sign of one of them. P_{int} is given by (A3.1) in which

$$R \equiv V(t)/V_0 = (1/2)(\mathbf{x}_4 - \mathbf{x}_1) \wedge (\mathbf{x}_2 - \mathbf{x}_3)/V_0. \qquad \text{(A3.6)}$$

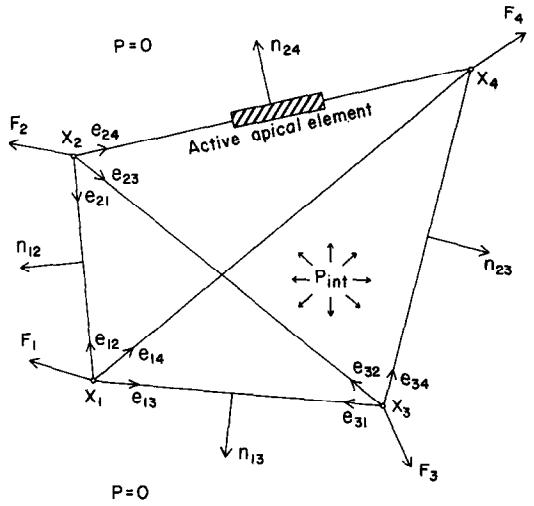

FIG. 14. Cross-sectional model of a single cell (cf. Fig. 5), with vertices labeled externally applied forces, f_1, f_2, f_3, f_4, indicated, and various unit vectors used in deriving the equations of motion shown.

Using (A3.2), (A3.5) becomes

$$\sum_{\substack{j=1 \\ j\neq i}}^{4} \mu_{ij}\mathbf{e}_{ij}\frac{d}{dt}L_{ij} = \mathbf{F}_i + (1/2) \sum_{\substack{j=1 \\ j\neq i \\ \text{(exclude diagonals)}}}^{4} P_{\text{int}}L_{ij}\mathbf{n}_{ij} + \sum_{\substack{j=1 \\ j\neq i}}^{4} k_{ij}(\cdot)(L_{ij} - L_{0_{ij}})\mathbf{e}_{ij}. \qquad \text{(A3.7)}$$

Let $\mathbf{z}(t)$ be the vector whose eight components are the vertical and horizontal components of $\mathbf{x}_1$, $\mathbf{x}_2$, $\mathbf{x}_3$, and $\mathbf{x}_4$. Then $\mathbf{e}_{ij}$, $\mathbf{n}_{ij}$, L_{ij}, and P_{int} can all be expressed as nonlinear explicit functions of $\mathbf{z}$. When all quantities (except $\mathbf{F}_i$) in (A3.7) are so expressed, (A3.7) can be put into the following form:

$$\sum_{l=1}^{8} A_{ml}(\mathbf{z})\frac{dz_l}{dt} = H_m(\mathbf{z}) + f_m(t), \quad \text{for} \quad m = 1, \ldots, 8, \qquad \text{(A3.8)}$$

in which each of the 64 components of the matrix A_{ml} and the 8 components of H_m are all explicit functions of $\mathbf{z}(t)$. The viscosity parameters, μ_{ij}, appear in the A_{ml}, and the elasticity modulii, $k_{0_{ij}}$, appear in the H_m. The rest length of the apical end, $L_{0_{24}}(t)$, also appears in the H_m. The eight-vector (f_m) holds the components of $\mathbf{F}_i$.

Equations (A3.8) do not, by themselves, determine $\mathbf{z}(t)$ because nothing in them precludes rigid body motions of the whole cell. We can, and must, fix the location of one of the $\mathbf{x}_i$, and also fix the orientation of one of

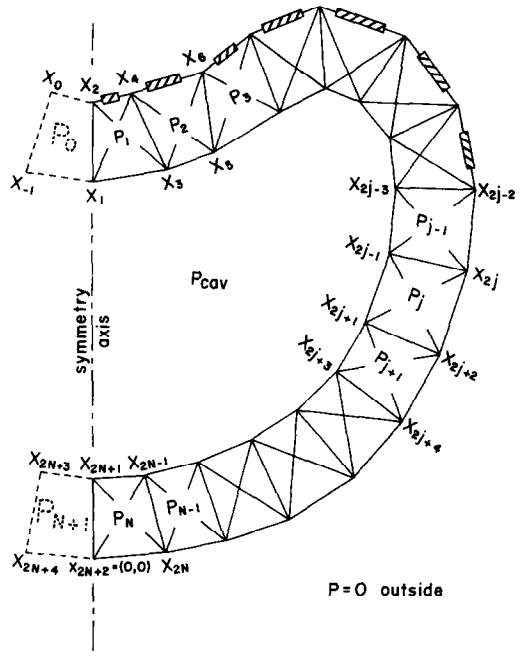

FIG. 15. A ring of cells showing labeling convention used for vertices and pressures in derivation of the equations of motion for the ring. The cells shown dashed, to the left of the symmetry axis, are mirrors of their immediate neighbors to the right.

the cell's edges joining that fixed node. Thus, we set $\mathbf{x}_1(t) = (0, 0)$, and, to make the basal end horizontal, we set $\mathbf{x}_3(t) = (x_3(t), 0)$. These constraints are $z_1(t) = z_2(t) = z_6(t) = 0$, and can be simply enforced by asserting $z_1(0) = z_2(0) = z_6(0) = 0$, and by replacing the jth row of (A3.8) by $dz_j/dt = 0$, for $j \epsilon \{1, 2, 6\}$. The resulting modified $\mathbf{A}(\mathbf{z})$ matrix is nonsingular, so that, given arbitrary values for $\mathbf{z}(t)$ and $f_m(t)$, the system of algebraic equations, (A3.8), can be solved uniquely for $d\mathbf{z}/dt$. The solution is obtained numerically, of course.

To complete the set of equations for a single cell, we add to (A3.8) the single equation, (6), that specifies how the rest length of the apical band, $L_{0_{24}}$, varies with time.

$$dL_{0_{24}}/dt = G(L_{24}, L_{0_{24}}). \qquad \text{(A3.9)}$$

The exact version we used of this equation is given as (A1.3) in Appendix 1. To make other elements of the cell active we would add a copy of (A3.9) for each mechanically triggerable strut.

The ODE system consisting of (A3.9) and (A3.8 modified) is rather time-consuming to treat numerically, because of its implicit nature; at each time step the components of the **A** matrix must be calculated from the new **z** values and then the linear algebraic system must be solved for $d\mathbf{z}/dt$.

Using a numerical integration of (A3.8) and (A3.9), with the external force components at the corners, $(f_m(t))$, assigned in various ways, we are able to test how a single cell responds to external tractions, and to discover, in particular, how much the apical surface must be stretched to be triggered.

In Appendix 4, we explain the way many copies of the single cell just modeled are assembled into a closed ring of cells to generate the simulations presented in this paper.

APPENDIX 4: MATHEMATICAL MODEL OF A RING OF CELLS

We describe here the equations governing the rings of cells shown in the simulation sequences in Figs. 7, 8, 9, and 10. Each simulation begins at time $t = 0$ with a circular ring of $2N$ cells, each of identical size and shape, with lateral edges lying along radii of the circle. The outer radius of the circle is 1 (this scales lengths) and the inner radius is $1 - h$. Thus, the model parameters N and h (= cell height) determine the initial geometry. We label the corners of the cells in the order shown in Fig. 15. We assume that the symmetry across the vertical midline persists from $t = 0$ into the future (this more than halves the computational complexity of the computer model). Thus, to describe the motion of the ring of cells, we must find $\mathbf{x}_1(t), \mathbf{x}_2(t), \ldots, \mathbf{x}_{2N+1}(t), \mathbf{x}_{2N+2}(t)\}$. We pin the lowest node, $\mathbf{x}_{2N+2}$, to (0, 0), and, by our symmetry assumption, $\mathbf{x}_1$, $\mathbf{x}_2$, and $\mathbf{x}_{2N+1}$ all have zero horizontal components. This means we must find $4N$-1 scalar coordinate functions of t. The initial values of these functions are determined by N and h. Further, by assuming that, at the initial instant, all the viscoelastic elements of all cells are stress free, N and h also determine all the rest lengths of all the spring elements. Each cell has the same volume, V_0, determined by N and h. $P_i(t)$, the internal hydrostatic pressure in the ith cell, is determined as explained in Appendix 3 [see Eq. (A3.1)]. The ambient outside fluid pressure is always zero. Let $\hat{V}(t)$ denote the amount of fluid in the internal cavity enclosed by the ring of cells. The pressure in this cavity fluid, $P_{\text{cav}}(t)$, is determined by Eq. (A3.1) in which we use $R_{\text{cav}} = V_{\text{cav}}(t)/\hat{V}(t)$, where $V_{\text{cav}}(t)$ is the actual volume of the cavity (computed from $\mathbf{x}_1, \mathbf{x}_3, \ldots, \mathbf{x}_{2N+1}$). In some simulations, we allow the cavity fluid to leak out (e.g., the simulation of gastrulation, cf. Fig. 7), and in others, $\hat{V}$ is held constant to simulate a leakproof internal cavity [e.g., in the simulations of neurulation (Fig. 9) and of ventral furrow formulation (Fig. 8)]. In cases when the fluid leaks out, we use

$$\frac{d}{dt}\hat{V}(t) = \beta(P_{\text{cav}} - 0)\left\{\begin{array}{l}\text{circumference of}\\ \text{inner boundary}\\ \text{of cavity}\end{array}\right\}. \qquad \text{(A4.1)}$$

$\mathbf{e}_{ij}$, $\mathbf{n}_{ij}$, L_{ij}, $L_{0_{ij}}$, μ_{ij}, k_{ij}, and T_{ij} have the same definitions here as in Appendix 3, and the equations of motion are obtained in the same way, by requiring that at each node, $\mathbf{x}_i$, the sum of all forces acting be zero. These equations are (since, now, no "external" forces act)

$$\sum_{j\in\psi_i} T_{ij}\,\mathbf{e}_{ij} + (1/2)\sum_{j\in\phi_i} \Delta P_{ij} L_{ij}\mathbf{n}_{ij} = 0,$$

$$\text{for} \quad i = 1, 2, \ldots, 2N+2, \tag{A4.2}$$

where the index sets ψ_i and ϕ_i are defined by

$$\begin{aligned}\psi_i &\equiv \{i-2, i-1, i+1, i+2, i+3\},\\ &\quad \text{when } i \text{ is odd,}\\ &\equiv \{i-3, i-2, i-1, i+1, i+2\},\\ &\quad \text{when } i \text{ is even.}\end{aligned} \tag{A4.3}$$

$$\begin{aligned}\phi_i &\equiv \{i-2, i+1, i+2\},\\ &\quad \text{when } i \text{ is odd,}\\ &\equiv \{i-2, i-1, i+2\},\\ &\quad \text{when } i \text{ is even.}\end{aligned} \tag{A4.4}$$

These index sets catalog exactly which other nodes $\mathbf{x}_i$ is connected to by a viscoelastic element.

In (A4.2), ΔP_{ij} is the pressure drop across the side between $\mathbf{x}_i$ and $\mathbf{x}_j$ in the direction of $\mathbf{n}_{ij}$, computed using the above definitions of the various pressures, all of which are calculated, using Eq. (A3.1), from ($\mathbf{x}_1$, $\mathbf{x}_2$, ..., $\mathbf{x}_{2N+2}$).

Using (A3.2), we put (A4.2) into the form

$$\sum_{j\in\psi_i} \mu_{ij}\,\mathbf{e}_{ij}\frac{d}{dt}(L_{ij}) = (1/2)\sum_{j\in\phi_i}\Delta P_{ij}L_{ij}\mathbf{n}_{ij} - \sum_{j\in\psi_i} k_{ij}(L_{ij}-L_{0_{ij}})\mathbf{e}_{ij},$$

$$\text{for} \quad i = 1, \ldots, 2N+2. \tag{A4.5}$$

We let $\mathbf{z}(t)$ be the vector, with $4N+4$ components consisting of the horizontal and vertical components of $\mathbf{x}_1(t), \ldots, \mathbf{x}_{2N+2}$. A few of the terms in Eq. (A4.5) reference the nodes $\mathbf{x}_{-1}$, $\mathbf{x}_0$, $\mathbf{x}_{2N+3}$, $\mathbf{x}_{2N+4}$ (see Fig. 15). These are obtained from $\mathbf{x}_3$, $\mathbf{x}_4$, $\mathbf{x}_{2N-1}$, $\mathbf{x}_{2N}$, using the symmetry constraint. That is, for example, if $\mathbf{x}_4 = (x_4, y_4)$, then $\mathbf{x}_0 = (-x_4, y_4)$. Also, when P_0 or P_{N+1} are referenced, by symmetry, we use $P_0 = P_1$ and $P_{N+1} = P_N$.

When $\mathbf{e}_{ij}$, $\mathbf{n}_{ij}$, L_{ij}, and ΔP_{ij} in (A4.5) are expressed explicitly in terms of the components of $\mathbf{z}(t)$, and the differentiation of L_{ij} is carried out, (A4.5) assumes the form

$$\sum_{l=1}^{4N+4} A_{ml}(\mathbf{z})\frac{dz_l}{dt} = H_m(\mathbf{z}), \text{ for } m = 1, \ldots, 4N+4. \tag{A4.6}$$

A_{ml} is a $(4N+4)$ square matrix of nonlinear functions of $\mathbf{z}$, but, using the nearest neighbor linkage pattern between nodes, expressed in the index sets in (A4.3) and (A4.4), A_{ml} is seen to be a banded matrix with band width 15. That is, only 15 stripes of components centered on the diagonal of A_{ml} are nonzero. Schematically

$(A_{ml}) =$ 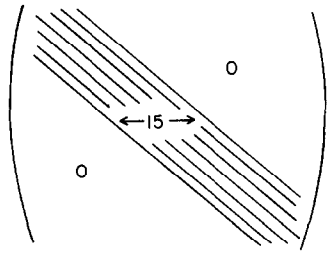

. (A4.7)

As in Eq. (A3.8), the μ_{ij} appear in A_{ml} ($\mathbf{z}$), the k_{ij} and $L_{0_{ij}}$ appear in $H_m(\mathbf{z})$, and the **A** matrix is singular until we modify it to preclude rigid body motions of the whole ring of cells. As explained above, we choose to set $\mathbf{x}_{2N+2} = (0, 0)$, and to pin the symmetry axis of the ring to the vertical coordinate axis by forcing $\mathbf{x}_1$, $\mathbf{x}_2$, and $\mathbf{x}_{2N+1}$ to have zero horizontal components. This we accomplish by setting $z_1(0) = z_3(0), = z_{4N+1}(0) = z_{4N+3}(0) = z_{4N+4}(0)$ to zero. Also, to force d/dt of each of these to be zero, we replace the jth row of (A4.6) by $dz_j/dt = 0$ for $j\epsilon\{1, 3, 4N+1, 4N+3, 4N+4\}$. This modification makes **A** nonsingular so that (A4.6), which are linear algebraic equations for the components of $d\mathbf{z}/dt$, can be solved uniquely (numerically only, in practice) for $d\mathbf{z}/dt$.

In each of the simulations presented in this paper, only a subset of the cells possess excitable apical filament bundles, namely cells number 1, 2, ..., $N_{\text{act}} < N$, where N_{act}/N differed slightly among the four simulations. ($N_{\text{act}}/N \approx 1/2$ approximately). Except for this distinction, all cells in a given simulation are identical. (A4.6) must be supplemented by N_{act} copies of Eq. (A1.3) which characterizes rest length changes in the active apical bands:

$$\frac{d}{dt}L_{0_{2i,2i+2}} = G(L_{2i,2i+2}, L_{0_{2i,2i+2}}),$$

$$\text{for} \quad i = 1, \ldots, N_{\text{act}}. \tag{A4.8}$$

Thus, finally, the equations of motion for the entire ring consist of (A4.1), (A4.6), and (A4.8). These number $4N + 4 + N_{\text{act}} + 1$ first-order ordinary differential equations. But five of them are void because, as explained above, z_1, z_2, z_{4N+1}, z_{4N+3}, and z_{4N+4} are all zero and their derivatives are zero as well. Thus the ODE integration algorithm must deal with $4N + N_{\text{act}}$ differential equations.

Note that no external forces act upon the ring of cells and that, because of the initial conditions we have set, the initial configuration of the ring is in equilibrium

(that is, no viscoelastic strut has any tension in it and all pressures are zero). Further, this initial state is stable to small perturbations, so nothing would change with time if integration of the equations proceeded from the initial state prescribed. To fire the starting gun, we trigger the apical filament band in cell No. 1 by setting $L_{0_{24}}$ to one-half of its equilibrium value. All simulations are begun this way, though, of course, there are many other provocations, including brief application of external loading, that could trigger the processes that unfold in Figs. 7, 8, 9, and 10.

We conclude with a brief description of the amount of computer work needed to integrate these equations, then give a table of parameter values used in the simulations of Figs. 7–10.

Numerical integration of the $4N + N_{act}$ ($\cong$142 in a typical simulation) coupled differential equations in (A4.1), (A4.6), and (A4.8) is moderately expensive in computer time. This is because the equations embedded in (A4.8) are implicit (the huge A matrix must be "inverted" at each time step) and turn out to be stiff [the larger Γ is in (A3.1) and the larger N is, the stiffer they become]. Only a well-tuned, implicit, multistep, ODE solver algorithm (with automatic step size adjustment to keep local errors below a specified tolerance) can cope with these equations. For the $N \approx 32$ and $N_{act} \approx 15$ values we used, even a small computer can hold the code needed for the simulations. It fits in a PDP 11/34, for example, but takes approximately 7½ hr per simulation (using a PDP 11/34 with a floating point processor).

On a PDP-10, each simulation requires about 25 min of CPU time. For completeness, we cite the parameter values we used to generate the simulations in Figs. 7, 8, 9, and 10. These parameter choices are not finely tuned; nearby parameter choices give "nearby simulations."

Parameter	Fig. 7 Gastrulation	Fig. 8 Ventral furrow	Fig. 9 Neurulation	Fig. 10 Exogastrulation
N = number of cells	32	32	32	30
N_{act} = number of active cells	14	8	13	16
h = cell height (fraction of outer radius)	0.13	0.3	0.13	0.12
β = cavity leakage parameter in Eq. (A4.1)	0.025	0.	0.	0.015
Γ = (cavity fluid compliance)$^{-1}$ in Eq. (A3.1)	400.	400.	400.	400.
Filament band trigger parameters in Eq. (A1.3)				
ϵ_1	0.07	0.06	0.1	0.2
ϵ_2	0.25	0.28	0.205	0.225
ϵ_3	0.35	0.35	0.4	0.4
γ	1.5	1.5	3.0	3.
Viscosity parameters in Eq. (A3.2)				
μ_{apical}	30.	30.	30.	30.
μ_{basal}	30.	30.	10.	10.
μ_{sides}	100.	50.	200.	200.
$\mu_{diagonals}$	40.	40.	40.	40.
Elasticity modulii in Eq. (A3.2)				
$k_{0_{apical}}$	25.	25.	25.	25.
$k_{0_{basal}}$	20.	3.	10.	10.
$k_{0_{sides}}$	20.	10.	20.	20.
$k_{0_{diagonals}}$	5.	5.	15.	15.

This research was partially supported by the following grants: NSF Grant MCS79-03548 to Odell; NSF Grant DEB7421240 to Oster; NIH Grant GM23959 to Burnside. The authors gratefully acknowledge numerous useful conversations with and comments from many colleagues, especially M. Bernfield, J. Bonner, E. Cox, A. Jacobson, J. Murray, L. Segel, M. Steinberg, N. Wessells, A. Winfree, and L. Wolpert.

REFERENCES

AXELSSON, J. (1971). Mechanical properties of smooth muscle, and the relationship between mechanical and electrical activity. *In* "Smooth Muscle" (E. Bulbring, A. F. Brading, A. W. Jones, and T. Tomita, eds.), pp. 289-315. Arnold, London.

BAKER, P. C., and SCHROEDER, T. E. (1967). Cytoplasmic filaments and morphogenetic movement in the amphibian neural tube. *Develop. Biol.* **15**, 432-450.

BERNFIELD, M., and BANERJEE, S. (1978). The Basal Laimina in epithelial-mesenchymol morphogenetic interactions. *In* "Biology and Chemistry of Basement Membranes" (N. A. Kefalides, ed.). Academic Press, New York.

BRYANT, P., BRYANT, S., and FRENCH, V. (1977). Biological regeneration and pattern formation. *Sci. Amer.* **237**, 66-81.

BURNSIDE, B. (1973). Microtubules and microfilaments in amphibian neurulation. *Amer. Zool.* **13**, 989-1006.

CLARKE, M., and SPUDICH, J. A. (1977). Nonmuscle contractile proteins: The role of actin and myosin in cell motility and shape determination. *Annu. Rev. Biochem.* **46**, 797-822.

CONKLIN, E. (1932). The embryology of amphioxus. *J. Morphol.* **54**, 69-151.

COOKE, J., and ZEEMAN, E. (1976). A clock and wavefront model for control of the number of repeated structures during animal morphogenesis. *J. Theor. Biol.* **58**, 455-476.

COWAN, J. (1970). A statistical mechanics of nervous activity. *In* "Lectures on Mathematics in the Life Sciences." Amer. Math. Soc., Providence, R. I.

FRISTROM, D., and FRISTROM, J. (1975). The mechanism of evagination of imaginal discs of *Drosophila melanogaster. Develop. Biol.* **43**, 1-23.

FRISTROM, D., and CHIHARA, C. (1978). The mechanism of evagination of imaginal discs of *Drosophila melanogaster* (evagination of disc fragments). *Develop. Biol.* **66**, 564-570.

GIERER, A. (1977). Physical aspects of tissue evagination and biological form. *Quart. Rev. Biophys.* **10**, 529-593.

GOODWIN, B., and COHEN, M. (1969). A phase-shift model for the spatial and temporal organization of developing systems. *J. Theor. Biol.* **25**, 49-107.

GUSTAFSON, T., and WOLPERT, L. (1967). Cellular movement and contact in sea urchin morphogenesis. *Biol. Rev. Cambridge Philos. Soc.* **42**, 442-498.

HITCHCOCK, S. E. (1977). Regulation of motility in nonmuscle cells. *J. Cell. Biol.* **74**, 1.

HODGKIN, A. L., and HUXLEY, A. F. (1952). A quantative description of membrane exitation in nerve. *J. Physiol.* **117**, 500-544 (and 424-496).

HOLTFRETER, J. (1943). Properties and functions of the surface coat in amphibian embryos. *J. Exp. Zool.* **93**, 251-323.

JACOBSON, A. G., and GORDON, R. (1976). Changes in the shape of the developing vertebrate nervous system analyzed experimentally, mathematically and by computer simulation. *J. Exp. Zool.* **197**, 191.

KELLAND, J. (1977). Inversion in Volvox (Chlorophyceae). *J. Phycol.* **13**, 373-378.

KORN, E. D. (1978). Biochemistry of actomyosin-dependent cell motility—Review. *Proc. Nat. Acad. Sci. USA* **75**, 588-599.

LEWIS, W. (1947). Mechanics of invagination. *Anat. Rec.* **97**, 139.

MARSLAND, D. (1956). Protoplasmic contractility in relation to gel structure: Temperature-pressure experiments on cytokinesis and amoeboid movement. *Int. Rev. Cytol.* **5**, 199.

MEINHARDT, H., and GIERER, A. (1974). Applications of a theory of biological pattern formation based on lateral inhibition. *J. Cell Sci.* **15**, 321-346.

ODELL, G., OSTER, G., and BURNSIDE, B. (1981a). The mechanical Basis of Morphogenesis. II. Chemical signalling between cells. In preparation.

ODELL, G., OSTER, G., and BURNSIDE, B. (1981b). The mechanical basis of morphogenesis. III. Periodic thickening of Epithelial cells tethered to an underlying dermal cell mass as in the early formation of hair follicle, scale, feather, and tooth primordia. In preparation.

OSTER, G., ODELL, G., and ALBERCH, P. (1981). Mechanics, morphogenesis and evolution. *In* "Lectures on Mathematics in the Life Sciences, Some Mathematical Questions in Biology" (G. F. Oster, ed.), Vol. 13, pp. 165-255, Amer. Math. Soc., Providence, R. I.

PROSSER, L. C. (1974). Smooth muscle. *Annu. Rev. Physiol.* **36**, 503-535.

PURCELL, E. M. (1977). Life at low Reynolds number. *Amer. J. Phys.* **45**, (1), 3-11.

SNYDER, J. A., and MCINTOSH, J. R. (1976). Biochemistry and physiology of microtubules. *Annu. Rev. Biochem.* **45**, 699.

SOMMERBELL, D., LEWIS, J., and WOLPERT, L. (1973). Positional information in chick limb morphogenesis. *Nature (London)* **244**, 492-496.

SPOONER, B. S. (1975). Microfilaments, microtubules and extracellular materials in morphogenesis. *BioScience* **25**, 440.

TAYLOR, D. L., and CONDEELIS, J. S. (1979). Cytoplasmic structure and contractility in amoeboid cells. *Int. Rev. Cytol.* **56**, 57.

TURING, A. M. (1952). The Chemical Basis of Morphogenesis. *Phil. Trans. Roy. Soc.*, **237B**, 5-72.

TURNER, F., and MAHOWALD, A. (1977). Scanning electron microscopy of *Drosophila melanogaster* embryogenesis. *Develop. Biol.* **57**, 403-416.

VIAMONTES, G., and KIRK, D. (1977). Cell shape changes and the mechanism of inversion in Volvox. *J. Cell. Biol.* **75**, 719-730.

VIAMONTES, G. I., FOCHTMANN, L. J., and KIRK, D. L. (1980). Morphogenesis in volvox: Analysis of critical variables, preprint.

WADDINGTON, C. H. (1940). "Organism and Genes." Cambridge Univ. Press, Cambridge.

WOLPERT, L. (1969). Positional information and the spatial pattern of cellular differentiation. *J. Theor. Biol.* **25**, 1-47.

WRAY, J. S. (1979). Filament geometry and the activation of insect flight muscles. *Nature (London)* **280**, 325-326.